



Deposited via The University of Sheffield.

White Rose Research Online URL for this paper:

<https://eprints.whiterose.ac.uk/id/eprint/119830/>

Version: Accepted Version

Article:

Culache, G., Byfield, M.P., Ferguson, N.S. et al. (2017) Robustness of beam-to-column end-plate moment connections with stainless steel bolts subjected to high rates of loading. *Journal of Structural Engineering*, 143 (6). 04017015. ISSN: 0733-9445

[https://doi.org/10.1061/\(ASCE\)ST.1943-541X.0001707](https://doi.org/10.1061/(ASCE)ST.1943-541X.0001707)

Reuse

Items deposited in White Rose Research Online are protected by copyright, with all rights reserved unless indicated otherwise. They may be downloaded and/or printed for private study, or other acts as permitted by national copyright laws. The publisher or other rights holders may allow further reproduction and re-use of the full text version. This is indicated by the licence information on the White Rose Research Online record for the item.

Takedown

If you consider content in White Rose Research Online to be in breach of UK law, please notify us by emailing eprints@whiterose.ac.uk including the URL of the record and the reason for the withdrawal request.

1 Robustness of beam to column end-plate moment connections with
2 stainless steel bolts subjected to high rates of loading

3 G. Culache, M. P. Byfield, N. S. Ferguson, A. Tyas

4

5 **Abstract**

6 This paper presents an experimental investigation into end-plate beam column connections for
7 buildings. The work demonstrates that a four-fold increase in the energy absorbed to failure can be
8 achieved by replacing carbon steel bolts with their stainless steel counterparts. Experimental tests were
9 carried out under load control and these provided the opportunity to observe the time required for
10 connection fracture. Under quasi-static loading, connections tested with stainless steel bolts showed
11 clearly visible signs of distress prior to failure; whereas the carbon-steel bolted equivalents provided no
12 warning of failure prior to brittle fracture.

13 Experimental tests were carried out on bolts and these showed strain rate induced strength
14 enhancements. End-plate connections were also tested under high strain rates. Loading rate was not
15 observed to significantly affect the performance of stainless steel bolted connections. However, carbon-
16 steel bolted connections were observed to weaken under high strain rates, therefore dynamically
17 increased material properties did not always translate into increase connection strength. The design
18 strengths predicted using Eurocode 3 were found to be in good agreement with the experimentally
19 observed values under quasi-static loading for both bolt types. Under high-strain rate conditions the
20 Eurocode 3 method was also found to provide a good prediction for stainless steel bolted connections;
21 but was found to over predict for carbon-steel connections.

22 The simple modification of replacing carbon-steel bolts with their stainless steel equivalents is shown
23 to be an effective way of improving the performance of industry standard connections. This
24 modification is of relevance to the design of buildings and other structures in which the ductility is of
25 high importance, for example in structures which may need to resist transient loads from blast or impact.

26

27 **Introduction**

28 During World War II a considerable amount of research was carried out into weapons effects on
29 buildings by Lord John Baker and Sir Dermot Christopherson (Byfield 2006). Their forensic
30 investigations identified a distinct weakness in the beam-column connections used during that time in
31 multi-storey steel framed buildings. They concluded that the majority of collapses caused by bombs
32 could be traced back to connection failures (Byfield 2006; Smith et al. 2010) and one of their main
33 recommendations was that full-moment joints should be provided when blast resistance is required
34 (Smith et al. 2010).

35 The need for the adequate tying of load bearing members was highlighted by the partial collapse
36 of the Ronan Point apartment building in 1968, after which regulations were introduced in the United
37 Kingdom defining the tying forces that beam connections must be able to resist without fracture. The
38 objective was two-fold: to help keep members tied together when subjected to lateral loads; and to
39 enable columns to be supported by catenary action in the event of column damage. The importance of
40 providing adequate tying was well known to World War II investigators, who often observed beam-
41 column connection failures occurred due to the suction pressures which develop when bombs detonate
42 near buildings (near misses) (Byfield 2006; Smith et al. 2010). The tie force regulation did not however
43 stipulate rotation requirements and it was subsequently demonstrated that the industry standard
44 connections used in most United Kingdom steel framed buildings lack the rotation capacity to support
45 columns through catenary action (Byfield & Paramasivam 2007). Despite this short-coming, the tie
46 force method remains popular with regulators and has been incorporated into Eurocode 1 (CEN 2005a).

47 The collapse of the World Trade Centre buildings in New York in 2001 led to a renewed interest
48 into improving the robustness of buildings. The aircrafts penetrated far enough that they adversely
49 affected the emergency exits blocking occupants in the upper stories of the towers and initiating the
50 collapse of the structures (Federal Emergency Management Agency 2002; National Commission on
51 Terrorist Attacks 2004). These events and others in the past two decades led to reports summarising
52 that one of the key safety issues in tall buildings is vulnerability to progressive collapse and the
53 following major conclusion was consistently reiterated (Shyam-Sunder 2005; Federal Emergency

54 Management Agency 2002): *“This vulnerability is directly related to the strength, ductility and hence*
55 *the energy absorption capacity of the connections between the main structural elements.”* (Institution
56 of Structural Engineers 2002)

57 These events also led to an intensification of research activity on progressive collapse with an
58 increase in publications from 20 papers between 1992 and 2000 to over 450 papers between 2002 and
59 2012 (El-Tawil, S., Li, H., Kunnath 2014). As there is significant risk, cost and effort associated with
60 high-quality experimental testing and the fact that it is often carried out by organizations that restrict
61 publication of data, computational modelling and simulation represent the primary tools in this research
62 area.

63 Whole frame numerical models which incorporate perfectly pinned or perfectly-rigid
64 connections have been shown to be inadequate when modelling progressive collapse (Stoddart 2012)
65 or blast structure interaction (Stoddart et al. 2013). Equally, using full three-dimensional connection
66 models with non-linear material models may create computational overload when used for modelling
67 whole frames dynamically. Representing connections as non-linear springs has also been shown to
68 present problems, because the horizontal forces which develop affect the joint stiffness, which cannot
69 be accounted for with a single non-linear spring element (Stoddart et al. 2013). This problem also occurs
70 during the modelling of frames subjected to fire, where thermal expansion, followed by catenary action
71 at higher temperatures induces high horizontal forces. This problem was overcome by Yu et al. (Yu et
72 al. 2009a; Yu et al. 2009b) who incorporated temperature dependent component models into whole
73 frame models. This avoids computational overload and was shown to accurately model experimentally
74 observed behaviour. This technique was subsequently shown to work for modelling progressive
75 collapse and blast structure interaction modelling (Stoddart 2012), (Stoddart et al. 2013), but using
76 strain rate dependent material models based on the Malvar and Crawford constitutive model (Malvar
77 1998).

78 As specialist high-strain rate tests are costly, many investigations have relied upon
79 computational modelling in the absence of experimental work. The importance of physical tests was
80 recognised by El-Tawil et al. (El-Tawil, S., Li, H., Kunnath 2014) who stated that *“One of the greatest*
81 *needs at the moment is for high-quality test data at the component and subassembly levels. These tests*

82 *will provide the necessary data for validation of modelling tools and development of design guidelines”*
83 (El-Tawil, S., Li, H., Kunnath 2014).

84 The National Institute of Standards and Technology conducted a series of full-scale tests
85 supported by advanced numerical modelling of beam-column assemblies (Sadek et al. 2011). These
86 simulated column removal scenarios, with each assembly consisting of three columns and two beams.
87 Each was subject to vertical displacement of the centre column until failure under quasi-static loading
88 rates (Lew et al. 2013). The novelty was in the creation of an improved connection with a reduced beam
89 section in its proximity. This improved ductility, increased ultimate deflections and loads. Reduced
90 finite element models, where three dimensional components were replaced with an assembly of
91 simplified two dimensional elements and rigid links, achieved a high degree of accuracy without
92 computational overload (Sadek et al. 2013).

93 Izzuddin and Vlassis (Vlassis et al. 2008; Izzuddin et al. 2008) also mention the need for further
94 development in simplified modelling of connections and for the realistic representation of the nonlinear
95 response of various connection types under dynamic loading conditions. Structures subjected to blast
96 and to a lesser extent progressive collapse, are subjected to high strain rates, and these are known to
97 affect both the strength and ductility of the materials. For this reason high strain rate tests are particularly
98 useful when investigating the performance of structures subjected to blast. It is generally accepted that
99 in the case of pure tensile testing of steel coupons and bars that the yield and ultimate stresses increase
100 with very high strain rates (Malvar 1998; Meyers 1994). This increase can influence connection
101 behaviour and it can be modelled using the dynamic increase factor (DIF) for stress . Christopherson
102 (Christopherson 1945) warned against the general application of a dynamic increase factor for steel
103 material properties during design, because he found that dynamic properties lack reliability (Smith et
104 al. 2010).

105 Models for the dynamic increase factor (DIF) of yield stress with strain rate are available
106 (Malvar 1998), (Johnson & Cook 1983). However, the increase in strength with high strain rates is not
107 necessarily applicable to bolts tested under high strain rates, due to the fact that bolts may fail through
108 a variety of failure mechanisms such as thread stripping (Mouritz 1994). Mouritz was one of the first to
109 conduct investigations into the behaviour of bolt-nut assemblies under strain rates that varied from 10^3

110 5 s^{-1} in tensile testing to 10^3 s^{-1} . He concluded that as the strain rate increases the threads are increasingly
111 likely to fail at lower fractions of the shank strength. Research carried out by Munoz-Garcia et al.
112 showed that M20 grade 8.8 fail through thread stripping and that the strength decreased with increasing
113 strain rates (Munoz-Garcia et al. 2005). Their experimental study included strain rates up to 20 s^{-1} .
114 Munoz-Garcia et al. (2005) found that M12 grade A4-70 stainless steel bolts fail at the much larger
115 failure strain of 16% as opposed to the 2-3% strain at which black carbon steel bolts fail.

116 Tyas et al. (2012) developed a testing rig for the combined rotation-extension testing of
117 nominally-pinned steel beam to column joints at high rates of loading. Loading time scales varied
118 between a few milliseconds and several minutes. Results showed that simple flexible end plate
119 connections show a decrease in ductility when failed at high strain rates.

120 Experimental tests were carried out at the University of Coimbra on T-stub components
121 subjected to impact loading (Barata et al. 2014) and numerical models were created that accurately
122 captured behaviour at both low and high strain rates (Ribeiro, Santiago, Rigueiro, et al. 2015), (Ribeiro
123 et al. 2016). Experimental tests and numerical modelling were also carried out on moment connections
124 at low and high strain rates. The experiments show that the dynamic increase factor of the steel is
125 reflected on the resistance of the connection as a whole, giving the connection a higher moment capacity
126 (Ribeiro, Santiago & Rigueiro 2015). Experimental tests simulating a column removal scenario under
127 both low and high strain rates, 10^{-3} s^{-1} to 10^2 s^{-1} , were carried out at the Norwegian University of Science
128 and Technology (Grismo et al. 2015). These showed that a more symmetrical deformation mode was
129 obtained in the dynamic case leading therefore to an increase in the energy absorbed by the connection
130 in the dynamic case. In both cases, the aforementioned investigations always used two nuts on grade
131 8.8 bolts in order to avoid thread stripping as a bolt failure mechanism.

132 Experimental work in the area of moment connections so far focused on testing connection with 2 or 3
133 bolt rows (Simões da Silva et al. 2001; Simões da Silva et al. 2002; Ribeiro, Santiago, Rigueiro, et al.
134 2015; Kuhlmann et al. 2009; Grismo et al. 2015), see Fig. 1 (a). However, industry standard
135 connections of high moment capacity often consist of end plates with five or more bolt rows (SCI/BCSA
136 Connections Group 1995), see Fig. 1 (b). Thus the tests carried out in this investigation included 5 and
137 7 bolt rows in order to investigate the performance of connections with more than 3 bolt rows.

138 **Experimental programme**

139 This experimental test programme was designed to investigate the moment vs. rotation response of
140 end-plate connections under quasi-static loading, as well as high strain rate loading. This could be
141 from the demands imposed by the catenary action which follows sudden column removal in a building
142 or the higher rates of loading developed from blast waves. The load was maintained throughout all of
143 the tests in order to investigate the time to fracture.

144 *Connections tested and design methodology*

145 This investigation explored the behaviour of extended end-plate and flush end-plate beam to column
146 connections. Fig. 2 shows the dimensions of the connections tested. Each connection was tested with
147 either M12 grade 8.8 carbon steel bolts or M12 grade A4-70 stainless steel bolts. All end plates were
148 12mm thick. All bolts were tested with one nut only.

149 Every connection was tested both statically and dynamically leading to eight different testing
150 configurations. The details of each test are listed in Table 1. Loading times and loading rates were
151 recorded during the tests and used to estimate the strain rates involved in the testing, see Table 1.

152 The moment connections were designed in accordance with Eurocode 3 (CEN 2005b) using the
153 methodology presented in industry design guides (SCI/BCSA Connections Group 2013) and (CEN
154 2005b). The connections were dimensioned in order to obtain failure of the connection by either bolt
155 failure, yielding of the end plate, buckling of the bottom flange of the beam stub, or a combination of
156 these modes. The resistance of a bolt row is given by the resistance of the equivalent T-stub. The T-
157 stub can fail in three different modes as shown in Fig. 3:

- 158 ▪ In mode 1 through complete flange yielding
- 159 ▪ In mode 2 through bolt failure with flange yielding
- 160 ▪ In mode 3 through bolt failure

161 The compression resistance of the combined beam flange and web in the compression zone is $F_{c,fb,Rd}$.

162 Expressions for calculating the tensile forces in the T-stubs $F_{T,1-3,Rd}$ and $F_{c,fb,Rd}$ are provided in the

163 Eurocode (CEN 2005b). The predicted values for the tested connections together with the assumed

164 distributions are presented in Fig. 4. The design moment resistance of the connection ($M_{j,Rd}$) is given
165 by:

$$M_{j,Rd} = \sum_r h_r F_{tr,Rd} \quad (1)$$

166 where $F_{tr,Rd}$ is the effective design tension resistance of bolt row r , h_r is the distance from bolt row r
167 to the centre of the compression and r is the bolt row number.

168 The Eurocode (CEN 2005b) defines a partial-strength joint as one which has a design moment resistance
169 lower than the plastic moment of resistance of the connected beam or column. In all cases the calculated
170 moment capacity of the connections was less than the capacity of the beam. The extended end-plate
171 connection achieves 77-78% of the beam capacity, whereas the flush-end-plate only 47-48%, see Table
172 2. Consequently all connection types are classified as partial strength according to the Eurocode (CEN
173 2005b).

174 *Material properties*

175 Tensile tests on the bolts and steel coupons taken from the end plate steel were carried out at strain rates
176 $\dot{\epsilon}$ ranging from 0.001/s to 1/s, see Table 3. A purpose-built testing rig was designed for testing the bolts
177 in tension so that they have the same engaged length as in the connection tests and that would allow
178 these to be tested within the aforementioned range of strain rates. Force versus displacement curves for
179 carbon steel and stainless steel bolt tests are shown in Fig. 5 for selected strain rates. The bolts had an
180 engaged length, between the bolt head and the nut, of approximately 35mm and only one nut was used.
181 This engaged length corresponded with that used in the actual joint tests.

182 As long as one nut was used, carbon steel bolts were always observed to fail through thread stripping;
183 see Fig. 6. The force-displacement curves for black bolts show a steep rise followed immediately by a
184 steep decline. After the nut thread was stripped, the nut slid over the rest of the thread of the bolt,
185 providing very little resistance in the process. The average energy absorbed by a carbon-steel bolt is
186 0.48 kJ and the nut travels for less than 4mm in the static case before thread stripping commences and
187 the resistance decreases sharply.

188 The stainless steel bolts were always observed to fail through necking of the bolt shank and ductile
189 fracture of the neck; see Fig. 6. As a consequence the bolts absorb more energy, with the average being

190 1.13 kJ. The elongation in the static case was observed to be up to 16mm, providing more ductility than
 191 the carbon steel bolts. *This failure mode is counter-intuitive since the tensile area in the threaded region*
 192 *is smaller than the tensile area of the bolt body. This behaviour is explained by the local increase in the*
 193 *strength levels for austenitic grades by cold working of the thread during manufacture (SCI/EuroInox*
 194 *2006). This reference (SCI/EuroInox 2006) reported that the 0.2% proof strength is typically enhanced*
 195 *by a factor of 50% in the corners of the thread by cold forming. It is possible that shank failure was*
 196 *obtained due to the high local strength of the threaded region of austenitic stainless steel.* The failure
 197 mechanisms and the differences in ductility are consistent with research carried out by Munoz-Garcia
 198 et al. (Munoz-Garcia et al. 2005). Thread stripping as a failure mechanism for carbon steel bolts was
 199 also observed in tests at the University of Coimbra, Barata et al. (Barata et al. 2014), and at the
 200 Norwegian University of Science and Technology, Grimsmo et al. (Grimsmo et al. 2015).

201 It was observed that the strength of both bolt types increases with increasing strain rates.

202 The Johnson-Cook (1983) model defines the relationship between stress and strain rates:

$$\sigma = (\sigma_0 + K\varepsilon^n) \left(1 + C_0 \ln \frac{\dot{\varepsilon}}{\dot{\varepsilon}_0} \right) \left[1 - \left(\frac{T - T_r}{T_m - T_r} \right)^m \right] \quad (2)$$

203 where σ is the stress, σ_0 is the yield stress under static conditions, the constants K , n and m are material
 204 parameters, T_r is the reference temperature, T_m the melting point, $\dot{\varepsilon}_0$ the reference strain rate, and
 205 importantly here the C_0 parameter characterises the strain-rate dependence of stress.

206 Assuming a similar relationship is true for the ultimate bolt force, this model was used in a simplified
 207 form to inform on the C parameter and quantify the dynamic increase in the bolt force with strain rate.

208 Considering only strain rate dependence, the DIF was expressed as:

$$DIF_{bolt} = \frac{F_{dynamic}}{F_{static}} = 1 + C \ln \frac{\dot{\varepsilon}}{\dot{\varepsilon}_0} \quad (3)$$

209 where the C parameter characterises the strain-rate dependence of force.

210 The dynamic increase factor for ultimate force is plotted for corresponding strain rates in Fig. 7 for both
 211 bolt types. Logarithmic trend lines and their equations are shown on the graph together with the
 212 equivalent Johnson-Cook C parameters. The C parameters are 0.0047 and 0.0069 for carbon steel and
 213 stainless steel respectively.

214 With increasing strain rates, a decrease in ductility was observed in both bolt types. In the case of the
215 stainless steel bolts the fracture strain can be estimated using measurements of the initial radius and the
216 radius of the neck at fracture (Bao & Wierzbicki 2004). The relationship between the fracture strain
217 ratio and strain rate is shown in Fig. 8. The fracture strain reduces with increased strain rate.

218 Tensile tests were also carried out for steel coupons cut from the beam stubs and end plates for the same
219 range of strain rates. The stress-strain relationship for the S355 end plate steel is shown in Fig. 9 for
220 two selected strain rates. In the case of the S355 steel it was observed that the dynamic effect is greater
221 on the yield stress than on the ultimate stress, which is consistent with Malvar and Crawford (Malvar
222 1998).

223 *Connection test rig set-up*

224 Most tests of this kind are carried out under controlled displacement, allowing the load to reduce slowly
225 and failure to occur in a safe manner. In this investigation the load was maintained during failure and
226 arguably this more closely matches the loading experienced in a real structure.

227 A 3D diagram of the testing rig used to carry out the experimental tests is shown in Fig. 10. In
228 the *quasi-static* tests the pressure is released through a cylinder and slowly increased to push the piston
229 or loading ram. Load is applied through the loading ram at one end of the “*flying column*” and was
230 measured using a load cell; see Fig. 10. The term “*flying*” is used because the column is supported by
231 roller bearings and is free to slide freely as soon as the connection fractures. The loading rates,
232 approximate strain rates and video frames per second are shown in Table 1

233 Displacements were measured at five points using laser displacement gauges (LDGs), shown
234 schematically in Fig. 11. LDG1 and LDG2 measured the displacement of the “*flying column*” in the
235 direction of the loading ram. These measurements enabled calculation of the rotation α of the column.
236 LDG3 measured the axial displacement of the “*column*”. LDG4 and LDG5 were located to measure
237 displacements of the angles and these were used to calculate the rotation β of the angles.

238 From force and moment equilibrium, Fig. 12 (a), the connection force and moment are given by:

$$F_C = F_A \quad (4)$$

$$M_C = d \cdot F_A \quad (5)$$

239 where F_C and M_C are the connection force and moment, F_A is the load applied, and d is the distance
 240 between the loading ram and the centre of the moment connection. Distance d is equal to 1105mm in
 241 all tests. Fig. 12 (b) presents the load applied F_A versus time for test T2A to exemplify the general
 242 character of loading in quasi-static cases.

243 In the case of *dynamic* loading of the connection, inertia effects are no longer negligible. From force
 244 and moment equilibrium, Fig. 13 (a), the connection force is given by:

$$F_C(t) = F_A(t) \cdot \cos[\theta(t)] - F_I(t) = F_A(t) \cdot \cos[\theta(t)] - m_c \ddot{\delta}_c \quad (6)$$

245 where F_C is the connection force, F_A is the applied load, F_I is the inertia force, m_c is the mass of the
 246 flying column and extension piece and $\ddot{\delta}_c$ is acceleration of the centre of mass. Fig. 13 (b) presents the
 247 load applied F_A versus time for test T4 to exemplify of the general character of loading in dynamic
 248 cases.

249 In order to calculate the connection moment the equilibrium equation for moments is written so that
 250 inertia effects are taken into account resulting in the following equation:

$$M_C(t) = d_{cm1} \cdot F_A(t) \cdot \cos[\theta(t)] + d_{cm2} \cdot F_C(t) - I_{mc} \cdot \ddot{\theta}(t) \quad (7)$$

251 where M_C is the connection moment, d is the distance between the loading ram and the centre of the
 252 connection, d_{cm1} is the distance between the loading ram and centre of mass, d_{cm2} is the distance
 253 between the centre of mass and the centre of the connection, I_{mc} is the mass moment of inertia about
 254 the centre of mass and was calculated as 339kgm². It was observed in the experiments that both the
 255 column and the angle supports rotated; see Fig. 11 (b). This was considered and displacements were
 256 recorded at the ends of both. The rotations of the column α and angles β , and the relative rotation θ are
 257 given by:

$$\alpha = \tan^{-1} \left(\frac{\delta_1 - \delta_2}{d_{12}} \right) \quad (8)$$

$$\beta = \tan^{-1} \left(\frac{\delta_4 - \delta_5}{d_{45}} \right) \quad (9)$$

$$\theta = \alpha - \beta \quad (10)$$

258 where δ_1 and δ_2 are the displacements at the ends of the column, d_{12} is the distance between the two
 259 laser gauges pointed at the column, δ_4 and δ_5 are the displacements at the ends of the angles, and d_{45}

260 is the distance between the two laser gauges pointed at the angles. Fig. 14 shows the rotation of the
261 “flying column” α and of the supporting angles β in dynamic test T4. All subsequent graphs are plotted
262 versus the relative rotation θ .

263 **Results**

264 The strength, ductility and energy absorbed for each connection test is summarised in Table 4. The
265 design moment capacities do not include factors of safety, which were removed in order to more clearly
266 reveal the accuracy of the Eurocode 3 design expressions. There was a good agreement between the
267 predicted and experimental test results under quasi-static loading. Under dynamic loading the stainless
268 steel flush end-plate connection strengthened, as would be expected from the dynamic increase in
269 material properties discussed earlier. The stainless steel extended end-plate connection weakened under
270 dynamic loading, but still achieved the design strength. This connection failed by flange buckling and
271 this may have prevented a dynamic strength increase developing, although this is discussed in more
272 detail later. The experimental testing of carbon-steel bolts under high strain rates would suggest an
273 increase in strength of the connections under high strain-rate loading, although this was not observed.
274 In fact these connections were significantly understrength and this highlights the known reliability
275 problems when using dynamic increase factors for material properties for calculating design strengths
276 (Smith et al. 2010). Important from a robustness point of view, stainless steel bolted connections can
277 be seen to have absorbed approximately 4 times the energy of the carbon steel connections.

278

279 **Quasi-static connection tests**

280 Fig. 15 shows the moment rotation behaviour for the static tests with values of strength labelled at
281 selected points. The tests loaded the connections over a period of approximately 300 seconds, after
282 which failure occurred in less than 100 milliseconds. The carbon steel bolts reached their ultimate
283 strength with no significant plastic deformation of the end plate, after which they failed in a brittle
284 manner. This is evident both in the moment versus rotation relationships, where the maximum rotation
285 is found to be just over 1 degree, as well as from the photographs of the connections taken after failure.

286 The stainless steel bolts deformed plastically and this caused significantly more deformation in
287 the plate than for the carbon steel bolted connections, see Fig. 16. It is important to note that bottom
288 flange buckling was observed in the case of the extended end-plate connection with stainless bolts. The
289 compression flange buckles and plastic deformation spreads through the web in compression. Referring
290 to the possible failure modes of a T-stub in Fig. 3, the carbon steel bolts led to a mode 3 failure. Although
291 the stainless steel bolts have a lower ultimate strength than carbon steel bolts, they changed the T-stub
292 to a mode 2 failure due to their superior ductility. Thus, the ductility of stainless bolts is reflected in an
293 increase in the ductility of the connections.

294 **Dynamic connection tests**

295 When the connections were loaded dynamically the moment increases to a first initial peak value in a
296 time period of 4 milliseconds. In test T7, after the first peak, the resistance of the carbon steel bolted
297 connection plateaus for 6 milliseconds as the threads of the nut deform plastically, Fig. 17. Once the
298 deformation commenced the resistance of the connection decreased linearly to zero in less than 20ms.
299 As the high-speed digital camera frame rate was 500fps, the entire loading and failure was captured
300 with sufficient detail to understand the failure process. Fig. 17 shows three frames at the commencement
301 of thread stripping, during the process, and after most threads are completely stripped. The end plate
302 remains flat during this process.

303 In test T4 (the stainless steel bolted connection shown in Fig. 17) the extended end plate and bolts are
304 seen to deform plastically, resulting in a gradual increase in moment capacity. The frame captured at
305 22ms shows significant plastic deformation of the end plate, the bolts, and the asymmetrical buckling
306 of the compression flange. Moment versus rotation relationships are presented in Fig. 18 for the
307 extended end plate connection together with the static loading cases. This asymmetric buckling may be
308 the cause of the reduction in the dynamic strength of the extended end-plate connection. In comparison,
309 flange buckling did not occur in the flush end-plate connection. The absence of this failure mode may
310 have allowed the stainless steel flush end-plate connection to develop a dynamic strength increase, as
311 was expected from the bolt material property tests.

312 A similar sequence of events was observed for the dynamic tests of the flush end plate connections.
313 Several important differences must be noted in test T11 on the stainless steel bolted flush connection,

314 Fig. 19. Here there was no buckling of the bottom flange and this is the only test where a dynamic
315 increase in the moment capacity of the whole connection was observed, as Fig. 19 illustrates.
316 In the carbon steel bolted connections thread stripping leads to a rapid loss of connection strength. In
317 the case of the stainless steel bolted end-plate connections, the bolt ductility provides time for end-plate
318 deformation before final failure, allowing for greater overall connection ductility, as illustrated by the
319 difference between top row and bottom row of images in Fig. 17.

320

321 **Conclusions**

322 Experimental tests on bolts have been presented. These were carried out under quasi-static and elevated
323 strain rates. Carbon steel bolts are shown to fail through thread stripping, whereas ductile necking was
324 observed in stainless steel bolts. Both bolt types showed strength enhancement under elevated strain
325 rates, in a manner consistent with the literature. However, these strength enhancements did not always
326 translate into increased connection strength. The stainless steel bolted connections were found to absorb
327 the same amount of energy before failure under static and high strain-rate loading. They were also
328 shown to be able to achieve their design values of strength under high-strain rate loading. In comparison,
329 the carbon steel connections were found to be under-strength under high strain-rate loading; i.e. the
330 dynamic increase in material properties demonstrated in the bolt tests did not translate into increased
331 connection strength under high-strain rate loading.

332 The quasi-static experimental connection strengths showed good agreement with the Eurocode 3 design
333 strengths for carbon steel and stainless steel connections. During the quasi-static tests loading occurred
334 over a time period of 300 seconds, after which failure occurred in an explosive manner in less than a
335 $1/10^{\text{th}}$ of a second. The carbon steel bolted connections reached their ultimate strengths with no
336 observable plastic deformation, whereas failure was preceded by extensive plastic deformation in both
337 the bolts and the end-plates in the stainless steel bolted connections.

338 This research demonstrates that the simple replacement of carbon-steel bolts with their stainless steel
339 equivalent will improve strength, ductility and the ability to resist dynamic loading for the end-plate
340 beam-column connections investigated.

341 **Acknowledgements**

342 The investigators would like to thank the Defence Science and Technology Laboratory, part of the
343 Ministry of Defence (United Kingdom) for funding this research.

344 **References**

345 Bao, Y. & Wierzbicki, T., 2004. On fracture locus in the equivalent strain and stress triaxiality space.
346 *International Journal of Mechanical Sciences*, 46(1), pp.81–98.

347 Barata, P. et al., 2014. Experimental analysis of a T-stub component subjected to impact loading.
348 *Naples: EUROSTEEL*.

349 Byfield, M.P., 2006. Behavior and Design of Commercial Multistory Buildings Subjected to Blast.
350 *Journal of Performance of Constructed Facilities*, 20(4), pp.324–329.

351 Byfield, M.P. & Paramasivam, S., 2007. Catenary action in steel-framed buildings. *Structures and*
352 *Buildings*, 160(5), pp.247–257.

353 CEN, 2005a. *BS EN 1991-1-7:2006+A1:2014 Eurocode 1. Actions on structures. General actions.*
354 *Accidental actions*, European Committee for Standardization (CEN).

355 CEN, 2005b. *BS EN 1993-1-8:2005 Eurocode 3: Design of steel structures - Part 1-8: Design of*
356 *Joints*.

357 Christopherson, D.G., 1945. *Structural defence*, London.

358 El-Tawil, S., Li, H., Kunnath, S., 2014. Computational Simulation of Gravity-Induced Progressive
359 Collapse of Steel-Frame Buildings: Current Trends and Future Research Needs. *J. Struct. Eng.*,
360 140(SPECIAL ISSUE: Computational Simulation in Structural Engineering). Available at:
361 <http://ascelibrary.org/doi/abs/10.1061/%28ASCE%29ST.1943-541X.0000897>.

362 Federal Emergency Management Agency, 2002. *World Trade Center Building Performance Study.*
363 *FEMA 403.*, Washington, DC.

364 Grimsmo, E.L. et al., 2015. An experimental study of static and dynamic behaviour of bolted end-
365 plate joints of steel. *International Journal of Impact Engineering*, 85, pp.132–145. Available at:

366 <http://www.sciencedirect.com/science/article/pii/S0734743X15001554> [Accessed October 15,
367 2015].

368 Institution of Structural Engineers, 2002. *Safety in tall buildings and other buildings with large*
369 *occupancy*,

370 Izzuddin, B.A. et al., 2008. Progressive collapse of multi-storey buildings due to sudden column loss
371 — Part I: Simplified assessment framework. *Engineering Structures*, 30(5), pp.1308–1318.
372 Available at: <http://www.sciencedirect.com/science/article/pii/S0141029607002805>.

373 Johnson, G.R. & Cook, W.H., 1983. A constitutive model and data for metals subjected to large
374 strains, high strain rates and high temperatures. *Proc. 7th int. symp. on ballistics*, p.7.

375 Kuhlmann, U. et al., 2009. *Robust structures by joint ductility*, Brussels.

376 Lew, H.S. et al., 2013. Performance of Steel Moment Connections under a Column Removal
377 Scenario. I: Experiments. *J. Struct. Eng.*, 139(1), pp.98–107.

378 Malvar, L.J., 1998. Review of Static and Dynamic Properties of Steel Reinforcing Bars. *Materials*
379 *Journal*, 95(5), pp.609–616.

380 Meyers, M.A., 1994. *Dynamic Behaviour of Materials* 1st ed., Wiley-Interscience.

381 Mouritz, A.P., 1994. Failure mechanisms of mild steel bolts under different tensile loading rates. *Int J*
382 *Impact Eng*, 15(3), p.14.

383 Munoz-Garcia, E., Davison, J.B. & Tyas, A., 2005. Analysis of the response of structural bolts
384 subjected to rapid rates of loading. *4th European Conference on Steel and Composite Structures*,
385 *Eurosteel 2005*, C(4.10), pp.147–154.

386 National Commission on Terrorist Attacks, 2004. *The 9/11 Commission Report*,

387 Ribeiro, J., Santiago, A., Rigueiro, C., et al., 2015. Analytical model for the response of T-stub joint
388 component under impact loading. *Journal of Constructional Steel Research*, 106, pp.23–34.
389 Available at: <http://www.sciencedirect.com/science/article/pii/S0143974X14003241> [Accessed
390 March 15, 2015].

391 Ribeiro, J. et al., 2016. Numerical assessment of T-stub component subjected to impact loading.
392 *Engineering Structures*, 106, pp.450–460. Available at:
393 <http://www.sciencedirect.com/science/article/pii/S0141029615006811> [Accessed November 20,
394 2015].

395 Ribeiro, J., Santiago, A. & Rigueiro, C., 2015. Numerical assessment of beam-to-column steel joints
396 subjected to impact loading. In *Eighth International Conference on Advances in Steel Structures*.

397 Sadek, F. et al., 2013. Performance of Steel Moment Connections under a Column Removal Scenario.
398 II: Analysis. *J. Struct. Eng.*, 139(1), pp.108–119.

399 Sadek, F. et al., 2011. Testing and Analysis of Steel and Concrete Beam-Column Assemblies under a
400 Column Removal Scenario. *J. Struct. Eng.*, 137(SPECIAL ISSUE: Commemorating 10 Years of
401 Research since 9/11), pp.881–892.

402 SCI/BCSA Connections Group, 1995. *Joints in steel construction: Moment Connections*, The British
403 Constructional Steelwork Association/The Steel Construction Institute.

404 SCI/BCSA Connections Group, 2013. *Joints in steel construction: Moment-resisting joints to*
405 *Eurocode 3 (P398)*, The Steel Construction Institute and The British Constructional Steelwork
406 Association.

407 SCI/EuroInox, 2006. *Design manual for structural stainless steel* 3rd ed., Euro Inox and The Steel
408 Construction Institute.

409 Shyam-Sunder, S., 2005. *Federal Building and Fire Safety Investigation of the World Trade Center*
410 *Disaster: Final Report of the National Construction Safety Team on the Collapses of the World*
411 *Trade Center Towers (NIST NCSTAR 1)*,

412 Simões da Silva, L., Santiago, A. & Vila Real, P., 2002. Post-limit stiffness and ductility of end-plate
413 beam-to-column steel joints. *Computers & Structures*, 80(5-6), pp.515–531. Available at:
414 <http://www.sciencedirect.com/science/article/pii/S0045794902000147> [Accessed October 15,
415 2015].

416 Simões da Silva, L., Simões, R.D. & Cruz, P.J.S., 2001. Experimental behaviour of end-plate beam-
417 to-column composite joints under monotonical loading. *Engineering Structures*, 23(11),
418 pp.1383–1409. Available at:
419 <http://www.sciencedirect.com/science/article/pii/S0141029601000542> [Accessed May 6, 2015].

420 Smith, P., Byfield, M.P. & Goode, D., 2010. Building Robustness Research during World War II. *J.*
421 *Perform. Constr. Facil.*, 24(6), pp.529–535.

422 Stoddart, E.P., 2012. *Development of Component-based Connection Modelling for Steel Framed*
423 *Structures Subjected to Blast or Progressive Collapse*. Southampton: University of
424 Southampton.

425 Stoddart, E.P. et al., 2013. Strain rate dependent component based connection modelling for use in
426 non-linear dynamic progressive collapse analysis. *Engineering Structures*, 55(0), pp.35–43.
427 Available at: <http://www.sciencedirect.com/science/article/pii/S0141029612002854>.

428 Tyas, A. et al., 2012. A Methodology for Combined Rotation-Extension Testing of Simple Steel
429 Beam to Column Joints at High Rates of Loading. *Experimental Mechanics*, 52(8), pp.1097–
430 1109.

431 Vlassis, A.G. et al., 2008. Progressive collapse of multi-storey buildings due to sudden column loss—
432 Part II: Application. *Engineering Structures*, 30(5), pp.1424–1438. Available at:
433 <http://www.sciencedirect.com/science/article/pii/S0141029607003239>.

434 Yu, H. et al., 2009a. Development of a yield-line model for endplate connections in fire. *Journal of*
435 *Constructional Steel Research*, 65(6), pp.1279–1289. Available at:
436 <http://www.sciencedirect.com/science/article/pii/S0143974X08002824> [Accessed March 15,
437 2015].

438 Yu, H. et al., 2009b. Tying capacity of web cleat connections in fire, Part 2: Development of
439 component-based model. *Engineering Structures*, 31(3), pp.697–708. Available at:
440 <http://www.sciencedirect.com/science/article/pii/S0141029608003659> [Accessed October 26,
441 2015].

442

Test No.	End plate type	Section size	Bolts type	Loading	Loading time	Loading rate	Approx. strain rates in the bolts	Video frames per second
T1	Extended	305x102x25	CS	Static	300 s	0.40 kN/s	0.002/s	10
T2A	Extended	305x102x25	SS	Static	300 s	0.40 kN/s	0.002/s	500
T7	Extended	305x102x25	CS	Dynamic	40 ms	20 kN/ms	20/s	500
T4	Extended	305x102x25	SS	Dynamic	40 ms	20 kN/ms	20/s	8000
T5	Flush	305x127x37	CS	Static	300 s	0.40 kN/s	0.002/s	500
T6	Flush	305x127x37	SS	Static	300 s	0.40 kN/s	0.002/s	500
T8	Flush	305x127x37	CS	Dynamic	40 ms	20 kN/ms	20/s	500
T11	Flush	305x127x37	SS	Dynamic	40 ms	20 kN/ms	20/s	8000

443

Table 1: Experimental test programme (Note: CS denotes Carbon Steel, SS denotes Stainless Steel)

444

Plate type	Bolts type	Connection design moment capacity with safety factors $M_{j,Rd}$ (kNm)	Connection design moment capacity without safety factors $M^*_{j,Rd}$ (kNm)	Beam stub capacity $M_{c,Rd}$ (kNm)	Percentage of beam capacity
Extended	CS	84	117	150 kNm	78%
Extended	SS	83	115	150 kNm	77%
Flush	CS	76	105	215 kNm	48%
Flush	SS	73	101	215 kNm	47%

445

Table 2: Design moment capacities of tested connection types

446

Connection element	Material designation	Average yield stress, f_y (N/mm ²)	Average ultimate tensile stress, f_u (N/mm ²)
305x102x25 UKB	S355	440 N/mm ²	530 N/mm ²
305x127x37 UKB	S355	400 N/mm ²	520 N/mm ²
End plate, 12mm thick	S355	407 N/mm ²	560 N/mm ²
M12 carbon steel bolts	Grade 8.8	-	935
M12 stainless steel bolts	A4-70	-	891

Table 3: Measured quasi-static material properties

447

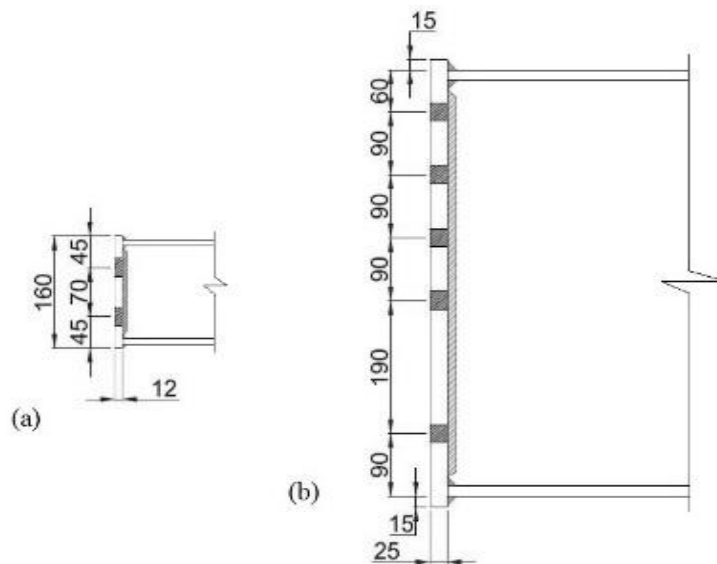
448

Test	Connection type	Bolt type	Loading type	Design capacity* M_{Rd} (kNm)	Experimental capacity M_{RExp} (kNm)	Rotation capacity φ_{exp} (°)	Absorbed energy E (kJ)
T1	Extended	Carbon steel	Static	117	127	1.20	2.0
T2A	Extended	Stainless steel	Static	115	133	4.22	8.3
T7	Extended	Carbon steel	Dynamic	117	90	0.70	2.5
T4	Extended	Stainless steel	Dynamic	115	115	4.40	8.3
T5	Flush	Carbon steel	Static	105	98	1.20	1.6
T6	Flush	Stainless steel	Static	101	105	3.42	6.9
T8	Flush	Carbon steel	Dynamic	105	87	0.80	1.8
T11	Flush	Stainless steel	Dynamic	101	115	3.50	6.9

449

Table 4: Connection test results (* calculated without safety factors)

450

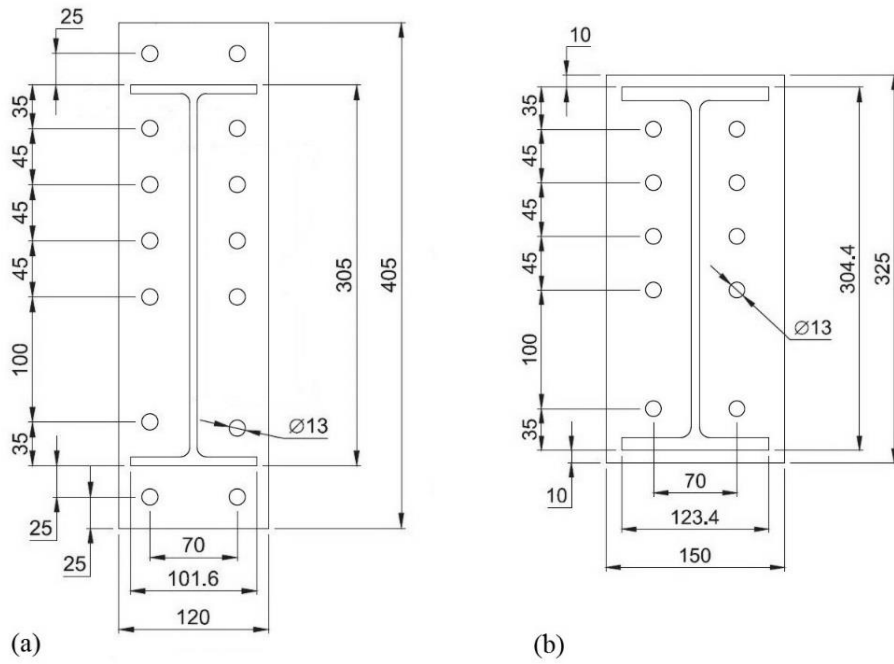


451

452

453

Fig. 1: (a) Connection tested at University of Liege (Kuhlmann et al. 2009) and (b) example of an industry-standard 5 bolt row connection (SCI, 1995)

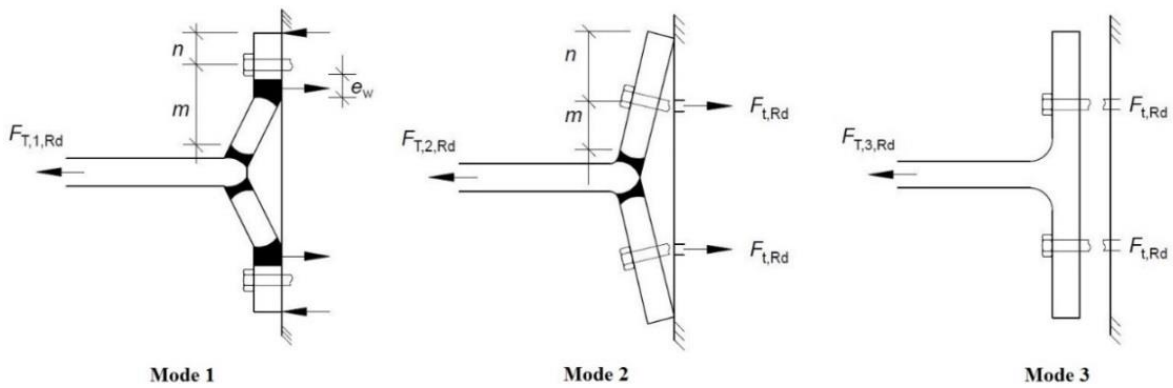


454

455

Fig. 2: Dimensions of (a) extended end-plate connection and (b) flush end-plate connection

456

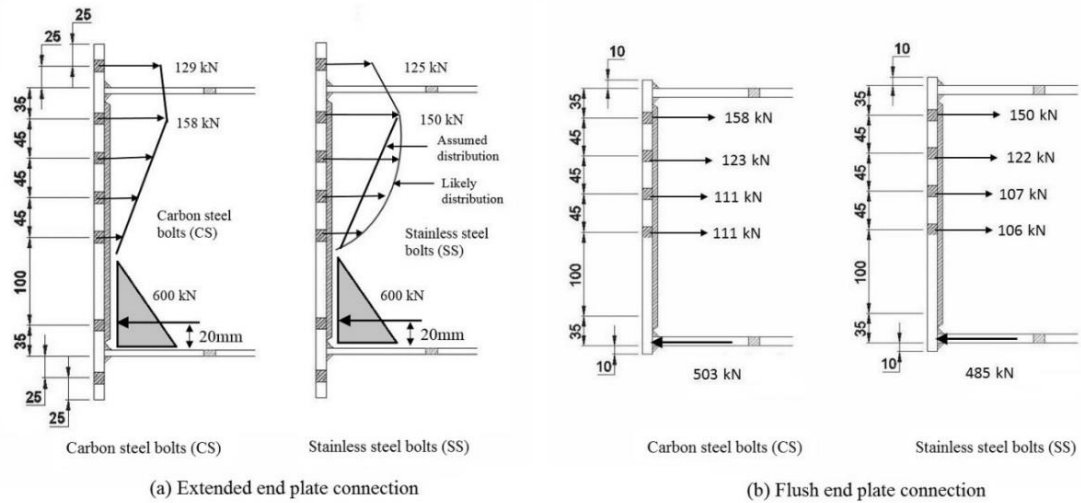


457

458

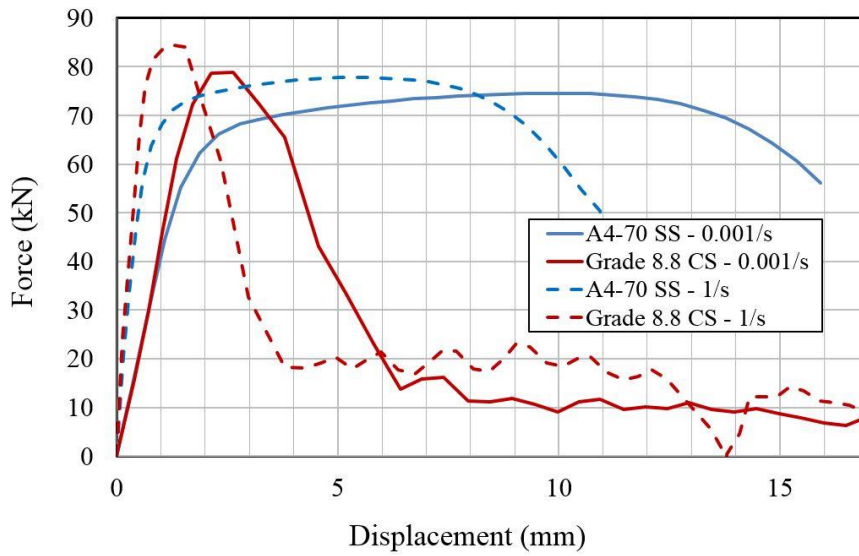
Fig. 3: Possible failure modes of the T-stub (SCI, 2013)

459



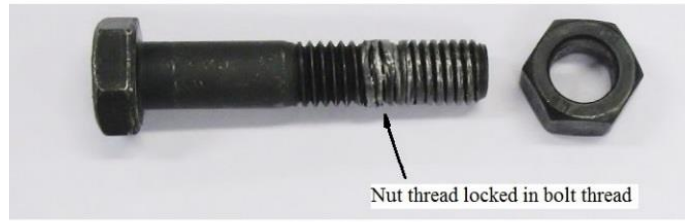
460
461
462

Fig. 4: Force distributions for the calculated design moment capacities



463
464
465

Fig. 5: Tensile tests of carbon steel (CS) and stainless steel (SS) bolts at selected strain rates



Carbon steel - failure by nut thread stripping

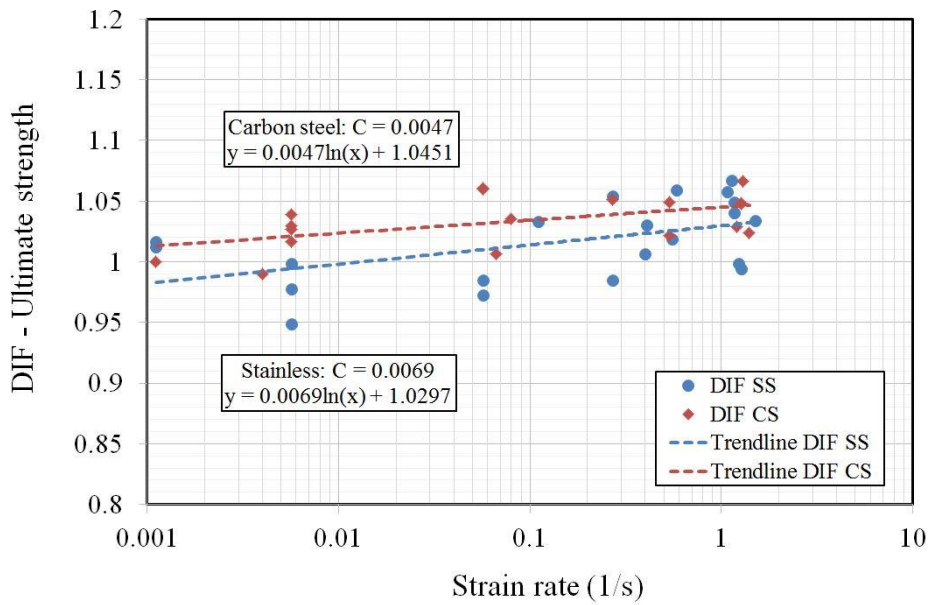


Stainless steel - failure by ductile body necking

466

467

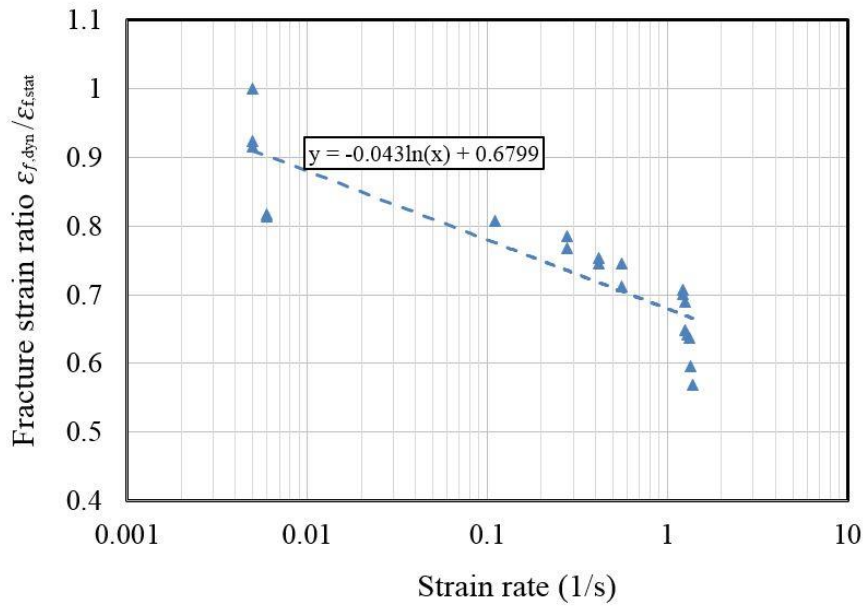
Fig. 6: Photos of failed bolts showing failure mechanism



468

469

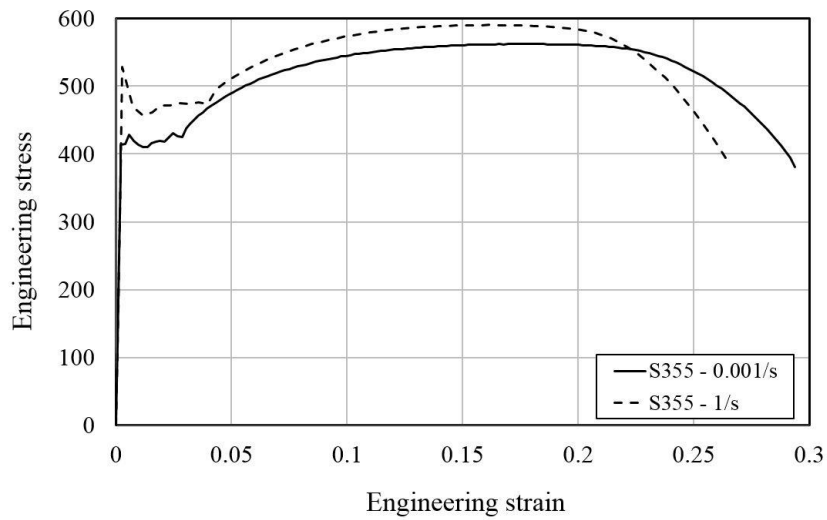
Fig. 7: Dynamic increase factor (DIF) versus strain rate from bolt tests



470

471

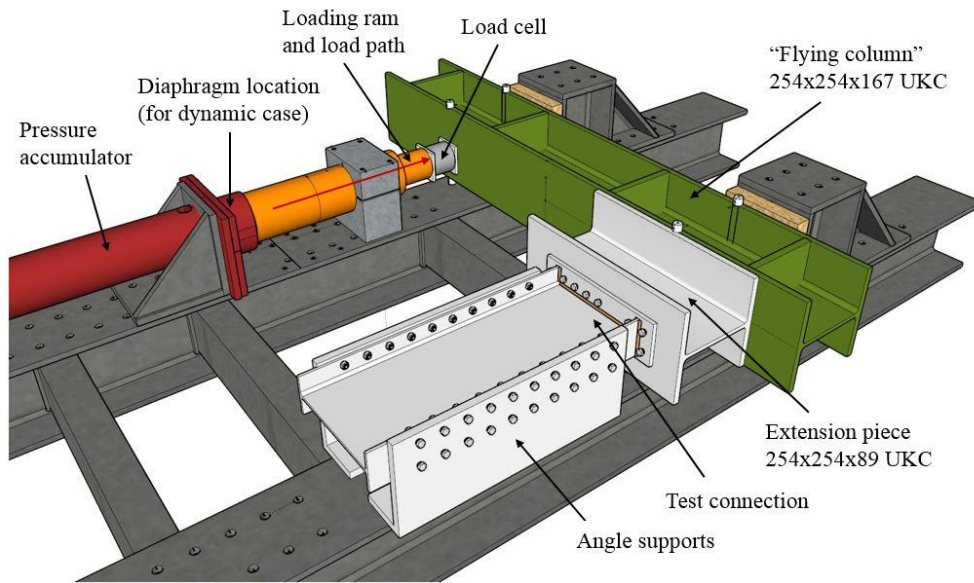
Fig. 8: Fracture strain ratio versus strain rate for stainless steel bolts



472

473

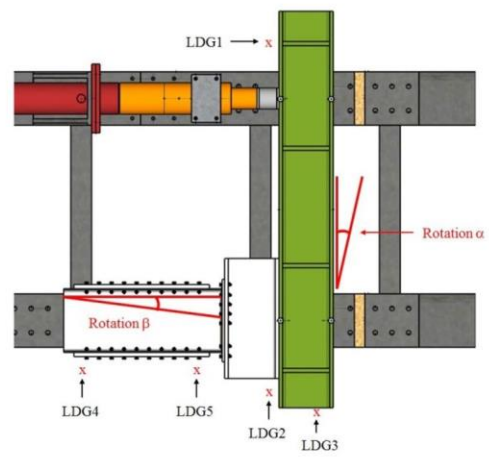
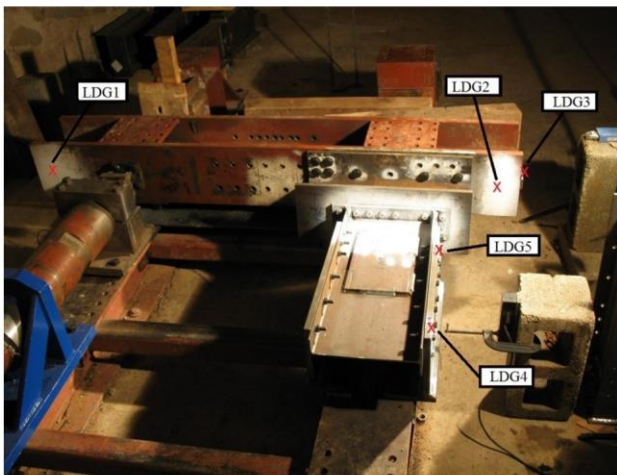
Fig. 9: Engineering stress strain curves for S355 steel taken from end plate for selected strain rates



474

475

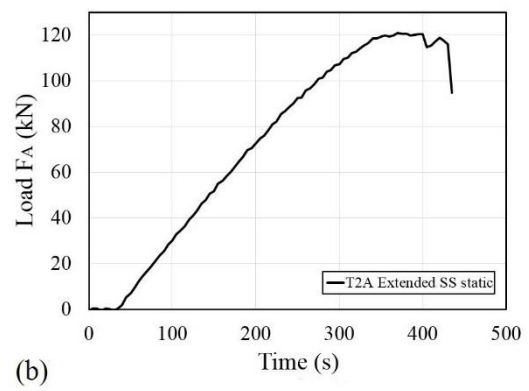
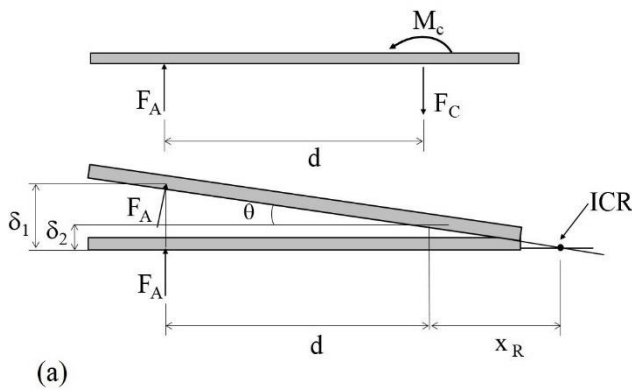
Fig. 10: 3D model of testing rig



476

477

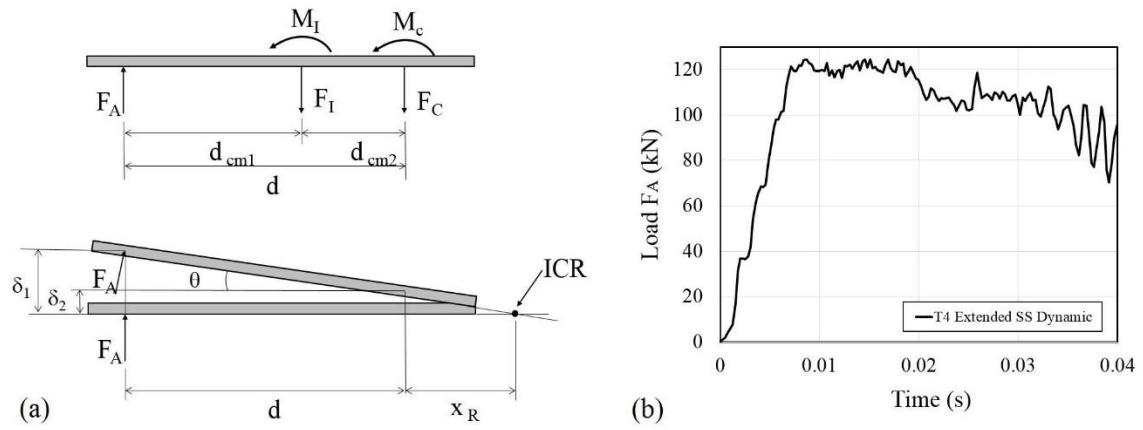
Fig. 11: Displacement measurement locations illustrated on (a) photo of rig and (b) 3D model



478

479

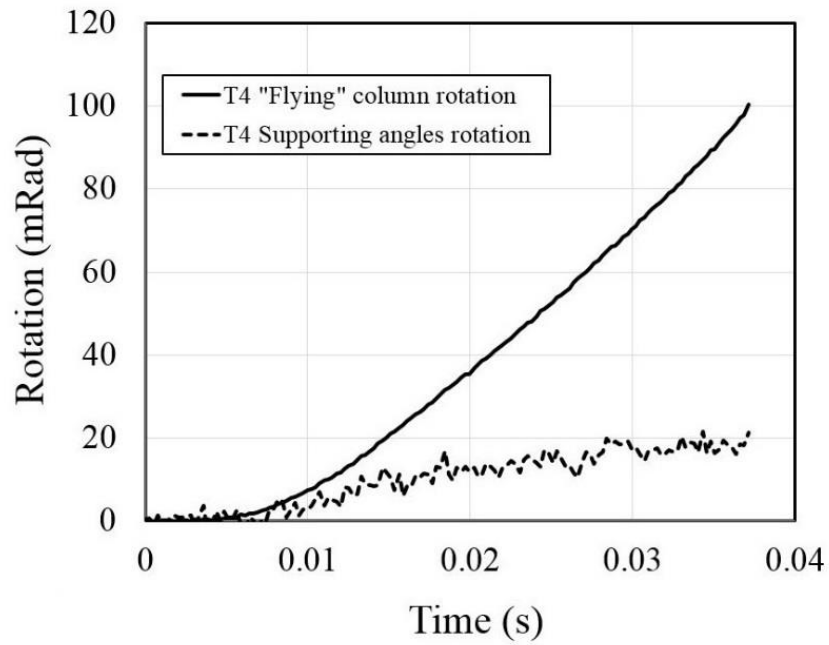
Fig. 12: Quasi-static loading scenario: (a) free body diagram and (b) test T2A load versus time



480

481

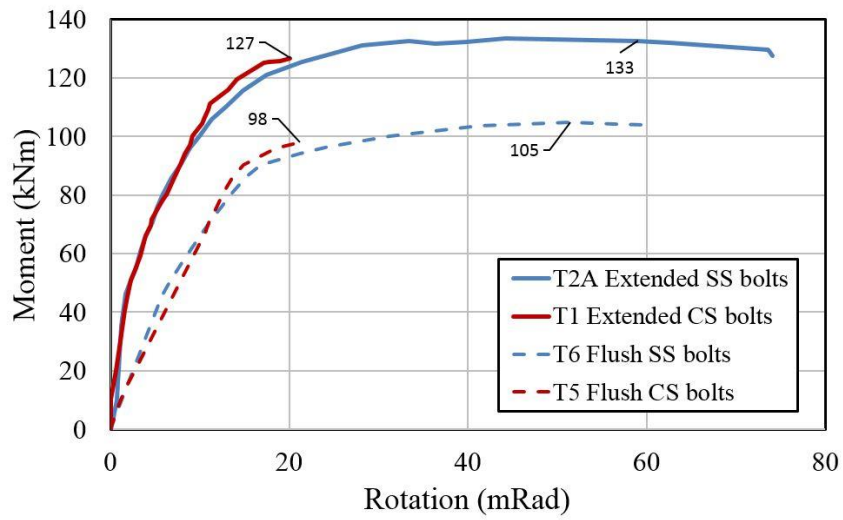
Fig. 13: Dynamic loading scenario: (a) free body diagram and (b) test T4 load versus time



482

483

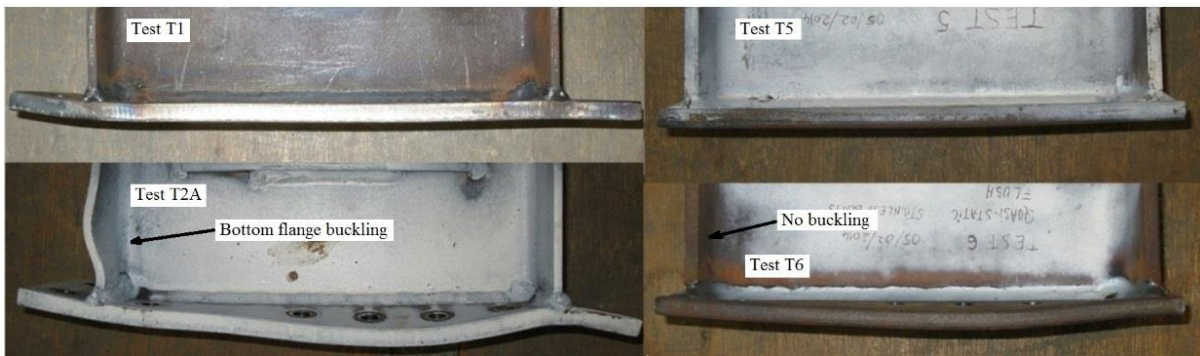
Fig. 14: Rotation versus time for dynamic test T4



484

485

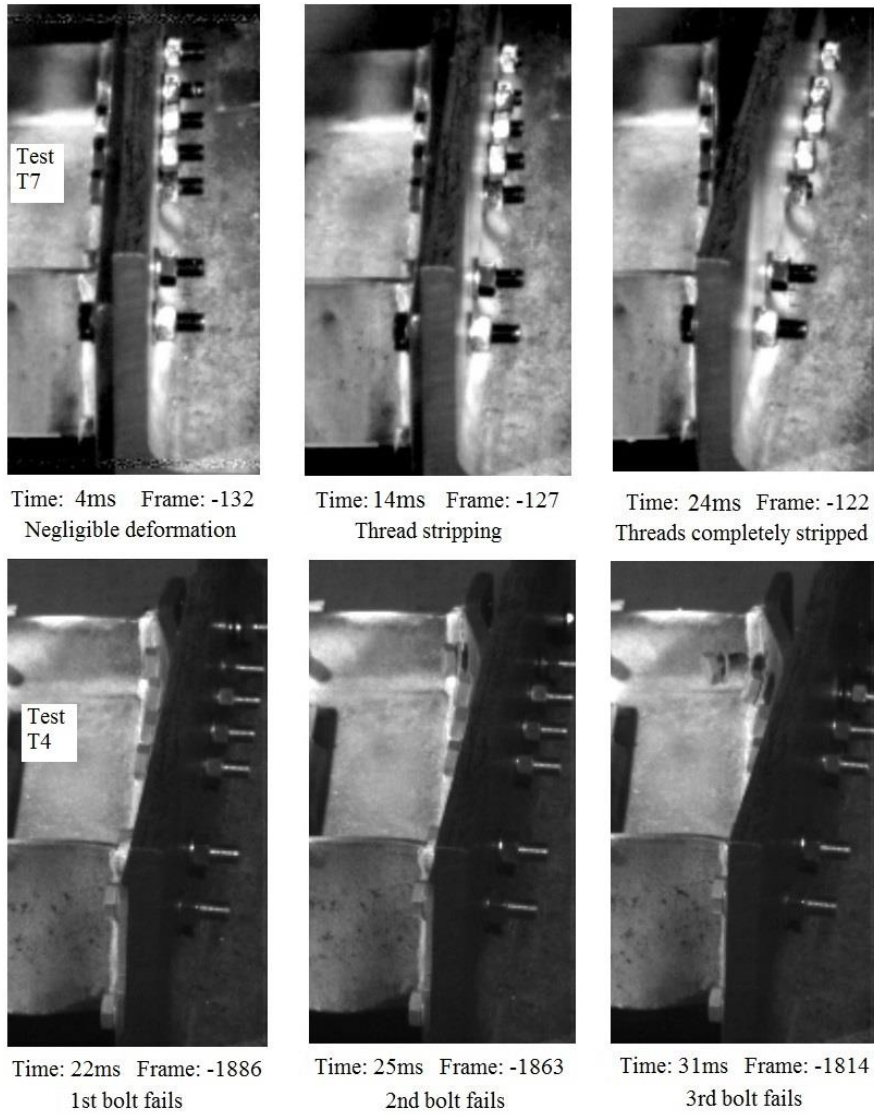
Fig. 15: Moment versus rotation for quasi-static tests



486

487

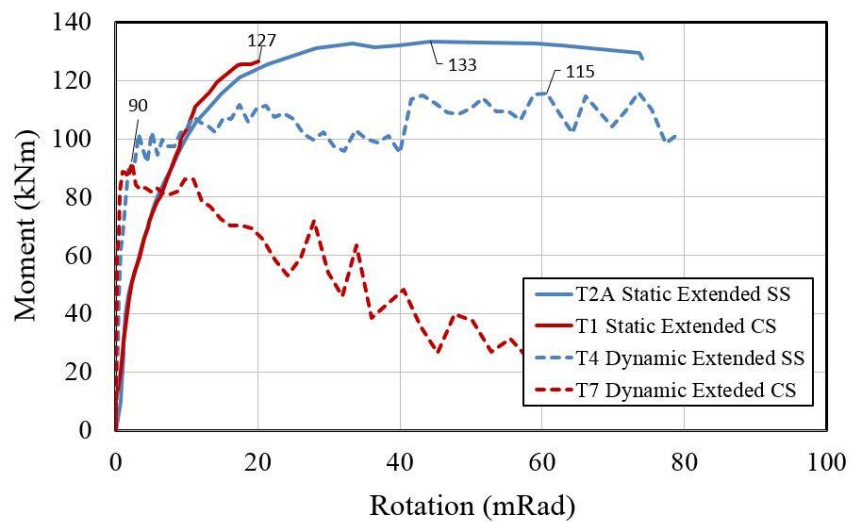
Fig. 16: Plate deformation with carbon steel (top) and stainless steel bolts (bottom) for quasi-static tests



488

489 **Fig. 17: Frames captured after commencement of dynamic loading for carbon steel bolted connection (top**

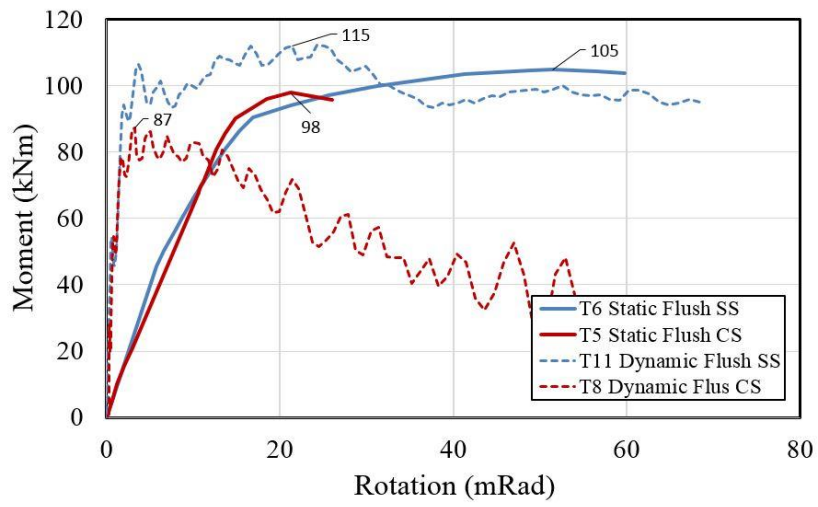
490 **row) and stainless steel bolted connection (bottom row)**



491

492

Fig. 18: Moment versus rotation for static and dynamic extended plate tests



493

494

Fig. 19: Moment versus rotation for static and dynamic flush plate tests

495

496

497